Monitoring the Behavior of the Shiadeh Earth Dam Using PLAXIS Software and Prediction Settlement with Radial Basis Function Algorithm

Seyed Razi Anisheh[1,a], Mohammad Sharifipour[1,b,*], Arash Azari[2,c]

[1] Department of Civil Engineering, Razi University, Kermanshah, Iran
[2] Department of Water Science and Engineering, Razi University, Kermanshah, Iran
*Corresponding Author: sharifipour@razi.ac.ir
a: ORCID 0000-0002-9761-0029, b:ORCID 0000-0002-7183-3291, c: ORCID 0000-0002-9643-3331

Abstract:

The specialized instruments installed in earth dams play a crucial and vital role in monitoring, controlling, and managing the structural stability of these dams against applied forces and destructive natural factors. In this study, the Shiadeh earth dam, Currently, all precision instruments installed on the dam are out of order, rendering it impossible to record any potential deformations or settlements. Therefore, this research focuses on predicting the dam's settlement during its operational phase, using historical data from the period when the instruments were fully functional and reliable. The prediction process was carried out using the advanced Radial Basis Function (RBF) algorithm. Within the scope of this study, both static and dynamic analyses were performed using the advanced PLAXIS 3D software to model the dam's behavior and evaluate its settlement along the crest. The settlement prediction results obtained through the RBF algorithm, when compared with ground survey data from micro-geodetic points located on the downstream slope of the dam, show acceptable agreement, confirming the validity and accuracy of the modeling approach employed. The analysis of crest settlement using PLAXIS 3D modeling indicates that throughout various reservoir impoundment conditions across different seasons, the dam maintained a high safety factor and demonstrated stable performance. The maximum recorded deformation at the dam crest was found to be 0.789 meters. Additionally, results from high-precision topographic surveying along the dam crest reveal that the settlement is not uniform, with the greatest amount of settlement occurring at a distance of 118.4 meters from the left abutment. In the three-dimensional PLAXIS model, the effect of the strike-slip fault was also taken into account, which led to intensified deformation.

Keywords:

Destructive natural, earth dam, specialized instruments, dynamic analyses, Radial Basis Function (RBF) algorithm, micro geodesic points

1- Introduction

Beiranvand (2024), shows that settlement in the dam's core gradually increases during the construction phase and stabilizes over time during the operational phase. Ghosh (2023), conducted a safety assessment of dams under static and seismic conditions using advanced soil and rockfill models and nonlinear analysis in PLAXIS 3D software. The analysis showed that seismic loading leads to plastic deformation and settlement of the dam, rather than slope failure.

Long-term settlement in well-compacted rockfill was found to be approximately 0.1 to 0.2% of the dam height. It was recommended to develop a risk framework and appropriate monitoring programs for better management of the dam's performance under seismic conditions. Research by De Alba, Seed (1978), shows that earth dams, due to their lack of rigidity, perform better in seismic conditions than concrete dams. Javdanian (2023), refers to the fact that in the field of hydraulics, experimental and statistical methods previously used in the construction of structures have gradually been replaced by numerical methods. A dataset of 103 earthquake-induced deformations in earth dams was analyzed. Using soft computing techniques such as feed-forward back-propagation and radial basis function neural networks, predictive models were developed to estimate slope deformations under varying seismic conditions. Chen (2014), after evaluating 670 earthquake-damaged earthen dams, found that cracking is the most common type of damage caused by earthquakes in these structures. Jamaluddin (2022), emphasized the importance of continuously measuring vertical and horizontal deformations using installed instruments to prevent the potential failure of the earth dam. Ambraseys (1967), noted that earlier studies suggested if bedrock lies at depth, a rigid foundation should be treated as flexible, though aspects of interaction were not explored. Idriss (1973), analyzed the response of a dam under periodic excitation in a semi-infinite environment. To investigate dynamic interaction, the following factors should be considered: a) Properties of the foundation material and the dam body, b) The ratio of the elastic modulus of the foundation to that of the dam body, c) The interaction between the dam and the foundation. Beiranvand et al (2021), The natural effect of earthquakes on earth dams has been the focus of many researchers studying the behavior of the dam. Kong (2018), considered relative settlement ratios between 0.4% and 1% as assessment limits for the dam crest, analyzing fragility when minor to severe failure occurred. Ding (2023) showed that the RBF neural network can be used to predict ground settlement caused by metro construction. In this study, data obtained from Structural Health Monitoring (SHM) were utilized, and the RBF model predicted ground settlement with high accuracy. This approach can assist engineers in better managing and designing civil engineering projects.

Jagan (2023) used the RBF network to predict soil deformation in underground excavations. The study demonstrated that the RBF network can model complex relationships between input parameters and soil deformations, making it an effective tool in geological and civil engineering analyses. Wang (2023) applied RBF neural networks to analyze the seismic behavior of structures. Using both simulated and real data, these networks were able to provide accurate predictions of the seismic response of structures, improving their design and safety. Zhang (2024) used RBF neural networks to predict the compressive and tensile strength of concrete reinforced with steel fibers. Various variables related to the steel fibers, including fiber length, diameter, and the water-to-cement ratio, were used as inputs to the network. The model accurately predicted the mechanical properties of concrete, which is significant for optimizing the design of high-performance and reinforced concrete. Wang (2024), combined RBF model has been used to predict the daily output power of photovoltaic power plants. In this model, various meteorological parameters such as solar radiation, wind speed, and ambient temperature are provided as inputs to the neural network, which is trained using the Whale Optimization Algorithm (WOA) to improve its performance. The results obtained demonstrate high accuracy in predicting the output power and can be applied to the optimal energy management of these power plants. This paper focuses on the monitoring and prediction of settlement in the Shiadeh earth dam using radial basis function (RBF) neural networks. The study highlights the advanced capabilities of these networks in accurately predicting complex parameters associated with settlement behavior. By integrating real-world data and computational techniques, the research provides a reliable framework for evaluating and forecasting dam performance under varying conditions, contributing to improved safety and maintenance strategies.

2- Aims and Methodology

In this study, three main steps were considered for monitoring settlement and assessing the dam's condition:

1. Field Investigations: In this phase, field surveys and ground mapping were carried out to perform leveling control using micro-geodetic points across seven sections on the downstream slope of the dam, as well as along the dam crest. The main objective of this stage was to collect precise data for comparison and validation of modeling results and subsequent analyses.

2. Settlement Prediction: In this section, the advanced Radial Basis Function (RBF) algorithm was used to predict settlement. The data used for this purpose were collected between the years 1999 and 2012 by precision instruments installed on the downstream slope of the dam. These instruments were in effective operation for 13 years, during which a total of 530 data points were recorded and measured. This dataset was specifically utilized to predict dam settlement in the year 2025, with predictions broken down by individual instrument data. An RBF approximation method based on Lagrange multipliers was presented by Fasshauer. This section provides a summary of its main characteristics. In this method, the problem is formulated as a constrained quadratic optimization, aiming to find an appropriate function to approximate the given dataset. The function is adjusted using Lagrange multipliers to achieve the best possible fit to the data and ensure high accuracy in approximation :

$$f(X)=\sum_{j=1}^{M} R_j \beta((\| X-Y_J \|), \qquad (1)$$

In this approach, the function $f(X)$ is constructed as a weighted sum of radial basis functions M (RBFs), each linked to a specific reference point Υ_J , and assigned a coefficient R_j. The goal is to determine the weight R=($R_1, \dots \dots, R_N)^W$ vector by minimizing the quadratic form:

$$f(X)=\frac{1}{2} R^W QR, \qquad (2)$$

Where Q is an M × M symmetric positive definite matrix. This minimization is subject to linear constraints SR=t , where S is an full-rank N × M matrix, and t=($t_1, \dots \dots, t_N)^W$ is a given vector. This optimization problem can be reformulated as a least-squares estimation (LSE):

$$f(R,U)=\frac{1}{2} R^W QR-U^W(SR-t), \qquad (3)$$

Here, U=($U_1, \dots \dots, U_N)^W$ represents the Lagrange multipliers, and the objective is to minimize (3) with respect to R both and U . This leads to solving the following system:

$$\frac{\partial F(R,U)}{\partial R}=QR-S^W U=0,$$
$$\frac{\partial F(R,U)}{\partial R}=SR-t=0, \qquad (4)$$

which, in matrix notation, takes the form:

$$\begin{pmatrix} Q & S^{W} \\ S & 0 \end{pmatrix}\begin{pmatrix} R \\ U \end{pmatrix} = \begin{pmatrix} 0 \\ t \end{pmatrix} \qquad (5)$$

Where $Q_{i,j}=\beta(\|\Upsilon_i - \Upsilon_j\|)$, and Q is symmetric. The solution to Equation (5) provides the final weights. To enhance computational efficiency, it is beneficial to minimize M, thereby reducing the cost of evaluating the approximated value $f(X)$ (Fasshauer,2007).

3. Static and Dynamic Analyses: Static and dynamic analyses of the earth dam were conducted using the advanced PLAXIS 3D software. These analyses took into account the lateral supports as well as the interaction effects between the foundation, dam body, and reservoir. During this process, all scenarios related to varying reservoir water levels across different seasons were evaluated in order to accurately assess the effects of static and dynamic loads on the dam's stability.

2.1- Site Selection (Inventory)

The Shiadeh earth dam, located 35 kilometers southwest of Babol city in Mazandaran Province, has been studied at the UTM coordinates x = 636028 and y = 4021865.The Shiadeh earth dam is located 35 kilometers southwest of Babol city in Mazandaran Province. According to ICOLD classification, the Shiadeh rockfill dam with a clay core is categorized as a high dam and is considered a significant structure. The dam's crest length is 450 meters, and its height from the riverbed is 33.0 meters. The dam was constructed in 1999 to supply irrigation water for downstream agricultural lands. Figure 1 illustrates the area of a landslide that occurred in 2004 at the downstream left abutment and the toe of the earth dam.

Fig. 1. Location of Shiadeh Earthen dam site

The layout plan of the piezometers, observation wells, and other geotechnical instruments—including inclinometers and settlement gauges—on the downstream slope of the Shiadeh earth dam is illustrated in Figure ۲ using solid circles along three cross-sections: A, B, and C.

These instruments have been continuously monitored and recorded since the commencement of the dam's operation.

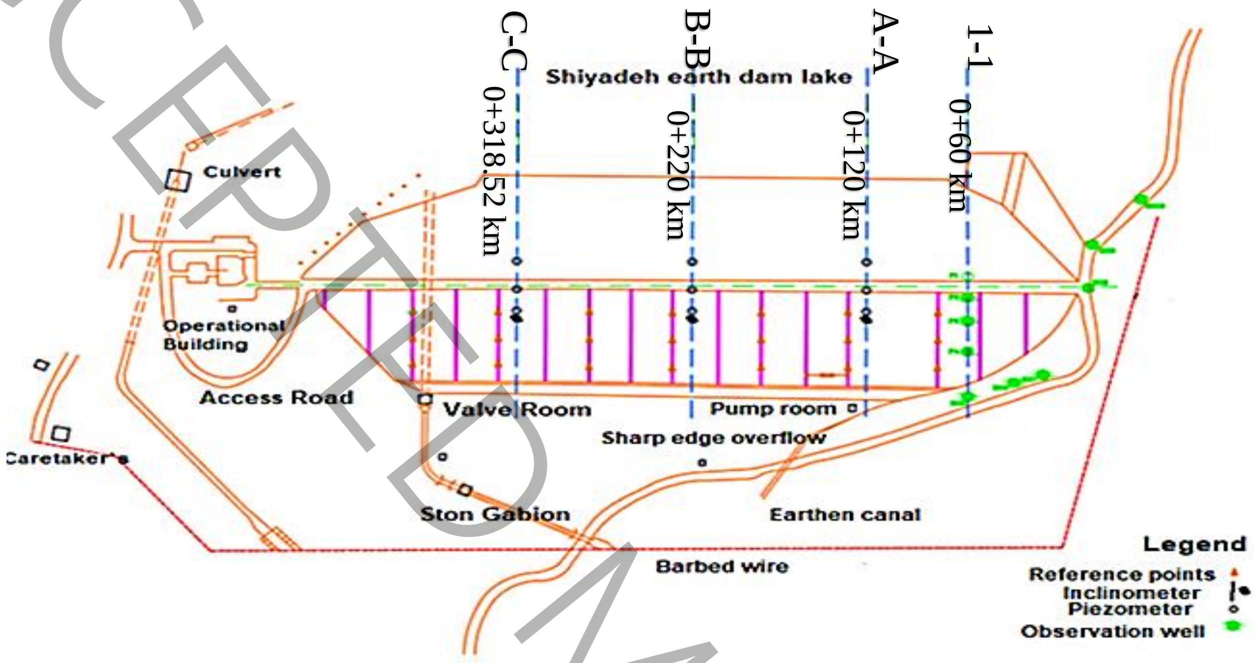

Fig.2. The layout plan of the instrumentation and observation well of the dam

The collected data has been systematically measured and documented over time. Furthermore, the accuracy and functionality of these instruments have been confirmed by the dam operation unit under the supervision of the Mazandaran Regional Water Authority. All installed instruments operated flawlessly and were fully functional from the start of the dam's operation on August 9, 1999, until October 10, 2012. However, after 2012, all the installed instruments ceased to function, leaving only three operational piezometers. The main cause of the piezometer failures was the bending and deformation of the piezometer tube during the dam's operational period, which prevented the measuring sensor inside the piezometer borehole from moving freely. Consequently, accurate measurement of the water level was not possible. This issue disrupted the continuous and precise monitoring of pore water pressure within the dam. To resolve this problem and continue the monitoring process, the Mazandaran Regional Water Company has drilled observation wells on the left bank of the dam site. Through these wells, changes in the water level can be measured directly and reliably, enabling effective monitoring of the dam's hydraulic Therefore, to monitor the dam, several observation wells were designed on the downstream slope and left abutment, and included in the execution plan.

In this study, a three-dimensional static and dynamic analysis was performed using PLAXIS software, considering the entire structure, foundation, and the interaction between the foundation and the embankment dam body. In Figure 3, the effective width required for the three-dimensional calculations is specified.

Anisheh and colleagues determined the effective width in terms of the height of a homogeneous embankment dam using PSO, CUCKOO, and IWO algorithms in a two-dimensional analysis with PLAXIS software.

All methods led to the same result, B = 1.81H. Therefore, in this study, the effective width was also considered in terms of height.

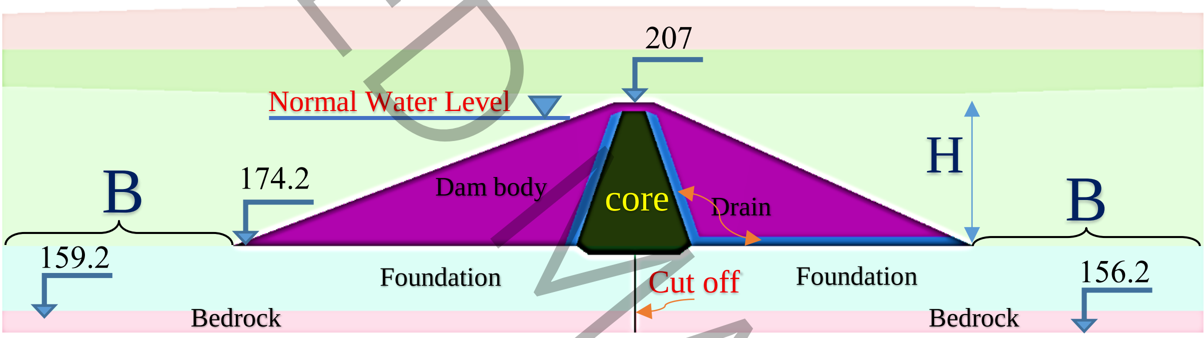

Fig.3. The effective width in the 3D model of an earth dam

In this study, the acceleration-time record of the Manjil earthquake was used for the dynamic analysis of the Shiadeh earth dam. One of the earthquakes that caused significant destructive effects in the Alborz region was the Manjil earthquake, which occurred in 1990 at the Abbar station. This earthquake recorded a peak ground acceleration (PGA) of 0.51g, a peak ground velocity (PGV) of 0.43 m/s, and a peak ground displacement (PGD) of 0.18 m. The magnitude of this event was Mb=7.3 and Ms=7.7, indicating the release of a considerable amount of seismic energy. In the seismic design of the Shiadeh earth dam, and based on an intended service life of 75 years, a design basis earthquake (DBE) with a moment magnitude (Mw) of 7.1 has been considered. Through the integration of results obtained from probabilistic seismic hazard analysis (PSHA), the expected ground motion parameters at the dam site have been estimated as follows: Peak Ground Acceleration (PGA) = 0.37g, Peak Ground Velocity (PGV) = 0.34 m/s and Peak Ground Displacement (PGD) = 0.16 m. By comparing these values with those of the Manjil earthquake, it is evident that all corresponding parameters for the Shiadeh dam design earthquake are lower. This indicates that the current design includes a reasonable safety margin, ensuring the dam’s stability under potential future seismic events of similar or lower intensity. To evaluate the interaction effects among the foundation, dam body, reservoir, and lateral supports as a single integrated system, the Manjil earthquake record was used for modeling in PLAXIS software (Figure ٤).

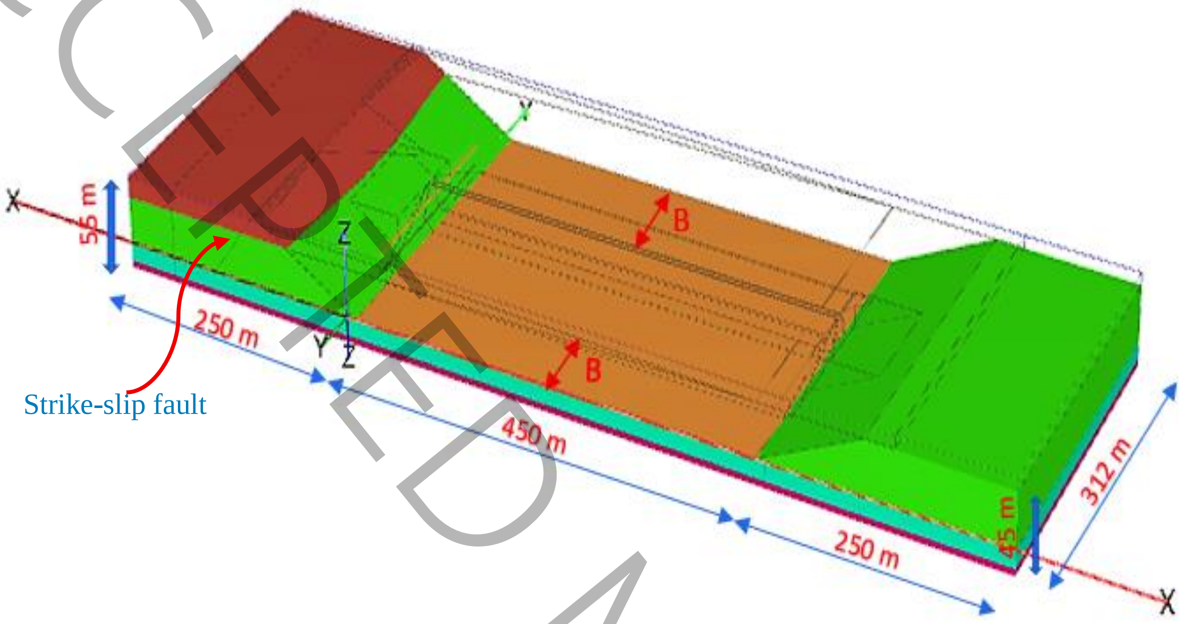

Fig. 4. The components of the body, supports, and the effective width

It should be noted that PLAXIS software is considered a reliable and suitable tool for solving dynamic analysis problems in modeling the dam body, foundation, and reservoir. One of the ways to identify a fault is by the presence of springs. Khoshraftar (2019), in a study on the relationship between faults and a karst spring in the Paraw–Bistoon area of Kermanshah, showed that the presence of springs within the study area can be an indicator for fault identification. The spatial distribution of springs obtained from the Mazandaran Regional Waer Company confirms the presence of a fault at the left abutment of the Shiadeh Dam site. A strike-slip fault was incorporated into the three-dimensional model along the entire left abutment, with a dip angle of 60 degrees relative to the horizontal (Figure 5).

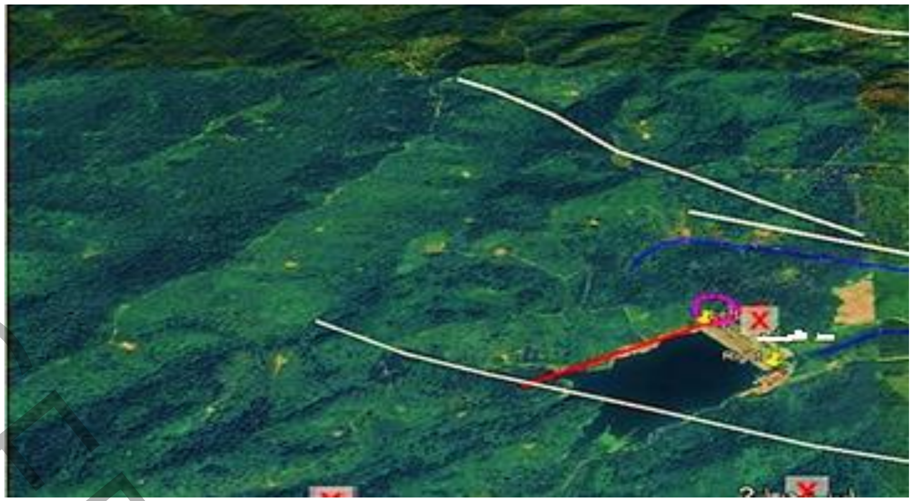

Fig. 5. Presence of a spring along the secondary fault

To determine the settlement and monitor the earth dam at the locations where the instrumentation has been installed, existing recorded data from the instrumentation over the years when they were functioning properly should be utilized. Subsequently, for trend analysis, by writing a program in MATLAB and using the powerful RBF algorithm, it will be possible to obtain the settlement values at the designated points. In the three-dimensional PLAXIS model, the interaction effects between the foundation, dam body, and reservoir were considered in an integrated manner. A fine mesh was applied to ensure high computational accuracy.

Table 1 presents the technical specifications of the earth dam. These specifications were prepared by the geotechnical consultant based on laboratory test results and were approved by Khazar Ab Consulting in 1998. The data provided in this table were used as the primary input for defining soil behavior and the parameters of the various components of the dam within the three-dimensional PLAXIS model.These parameters typically include the engineering and behavioral characteristics of geological layers, material properties, and the specifications of different structural sections of the dam, such as the clay core, filter layers, upstream and downstream shells, and other structural and protective components.

Utilizing this information enables an accurate simulation of the dam’s behavior and facilitates the assessment of its performance under different loading conditions.

Table 1. Characteristics of homogeneous Shiadeh Dam earth materials

Parameter	*Type*	*core*	*Filter*	*Shell*	*Left support layer*	*Right support Gravel*	*Riverbed Gravel*	*Impermeable layer*	*Cutoff & Retaining wall*	*Unit*
Behavioral Model	Model	Soft Soil	Hardening Soil	Hardening Soil	Soft Soil	Hardening Soil	Hardening Soil	Non porous	Liner Elastic	-
Type of Drainage	-	undrained	drained	drained	undrained	drained	drained	undrained	undrained	-
Specific weight above the water table	γ_{unsat}	18.8	18	21.8	17	21	21.2	22	25	KN/m^3
Specific weight at the groundwater table	γ_{sat}	19.8	20	22.2	19	21	22	22	25	KN/m^3
Young's Modulus	E	-	60E3	60E3	-	60E3	54E3	5000	23.5e6	KN/m^2
Shear Modulus	G	-	-	-	-	-	-	2174	10.22e6	KN/m^2
Poisson' Ratio	ν	0.2	0.2	0.2	0.15	0.2	0.2	0.15	0.15	-
Adhesion	C	50	2	2	16	10	2	150	-	KN/m^2
Internal Friction angle	Ø	19	30	35	17	24	34	25	-	-
Angle of Dilation	Ψ	0	0	5	0	0	4	0	-	-
Incremental Young's Modulus	E_{ur}	-	180E3	180E3	-	180E3	162E3	-	-	KN/m^2
Permeability Coefficient	K_x, k_y	0.864E-3	0.864	0.864	0.864E-3	0.0864	0.864	1E-6		m/day
λ^*	-	0.106	-	-	0.106	-	-	-	-	-
κ^*	-	0.055	-	-	0.055	-	-	-	-	-

3- Dynamic Analysis

One of the earthquakes with significant destructive effects in the Alborz region was the Manjil earthquake, which occurred in June 1990. Its magnitude was Mb=7.3 and Ms=7.7. The settlement of the earth dam was calculated using the 3D Plaxis software in 13 phases:

1. Initial phase: Existing state of the riverbed and the left and right abutments of the dam.

2. Phase 1: Excavation of the trench, construction of the retaining wall, and implementation of a cutoff to the foundation depth.

3. Phase 2: Construction of the earth dam.

4. Phase 3: Reservoir filling up to the maximum level (normal level).

5. Phase 4: Safety factor for a full reservoir.

6. Phase 5: Rapid drainage of the reservoir.

7. Phase 6: Safety factor for rapid drainage of the reservoir.

8. Phase 7: Slow drainage of the reservoir.

9. Phase 8: Safety factor for slow drainage of the reservoir.

10. Phase 9: Minimum water level in the reservoir.

11. Phase 10: Safety factor for Minimum water level in the reservoir.

12. Phase 11: Application of an earthquake to the earth dam after the construction is completed.

13. Phase 12: Application of an earthquake to the earth dam with a full reservoir up to the normal level.

Figure 6 shows the maximum acceleration of 0.28 g related to the normalized acceleration time history of the Manjil earthquake with the SEISMOSIGNAL 2022 software, which is considered under the maximum design level (MDL) and used in the modeling.

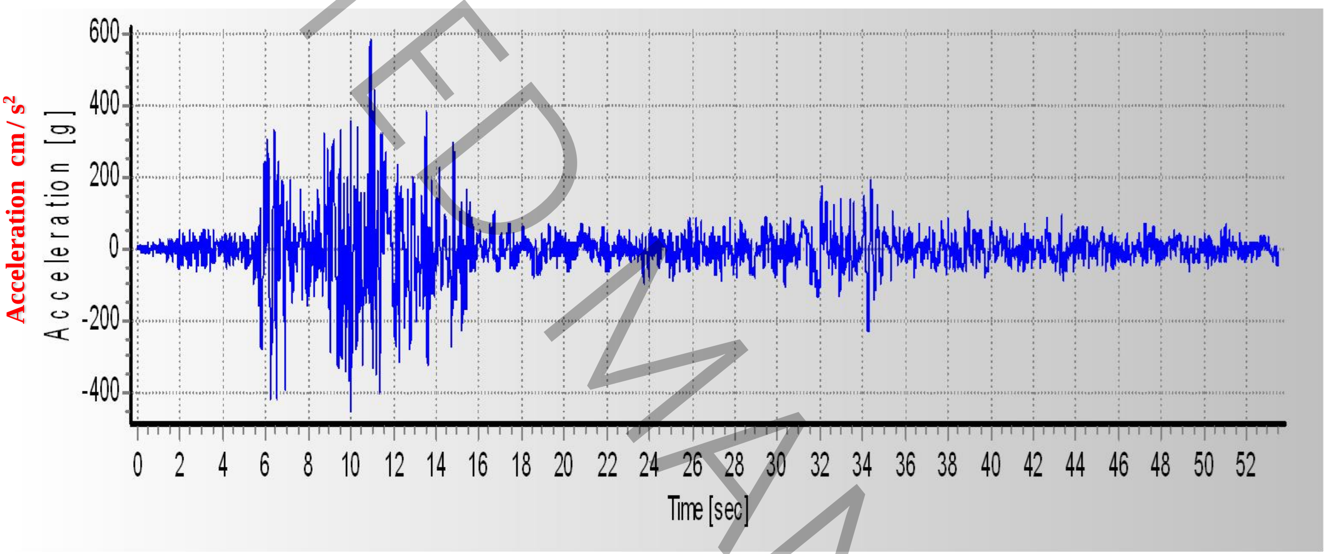

a)Acceleration mapping of the first component of the Manjil earthquake

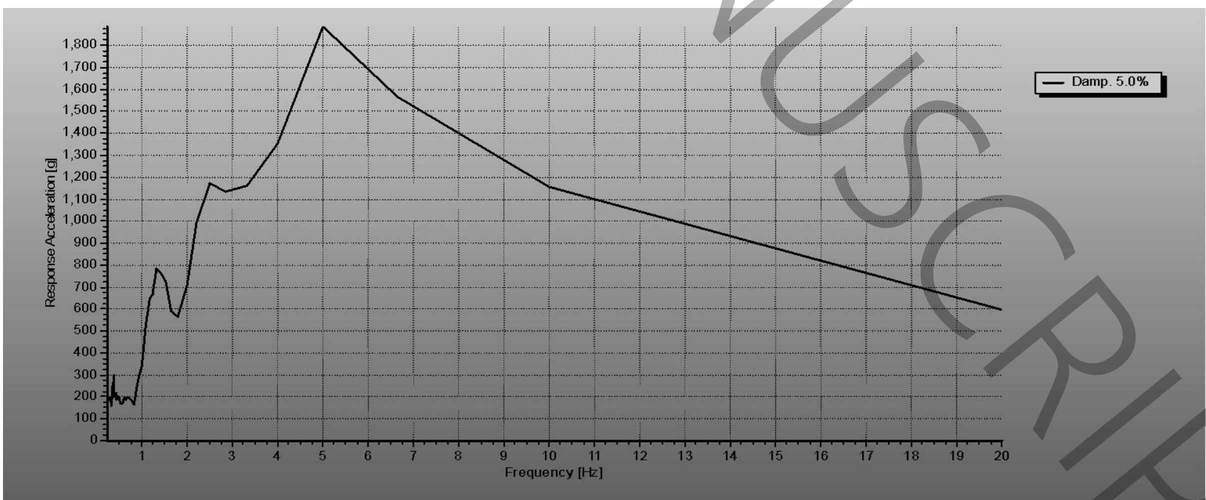

b) The acceleration response spectrum of the first component of the Manjil earthquake(Damping 5%)

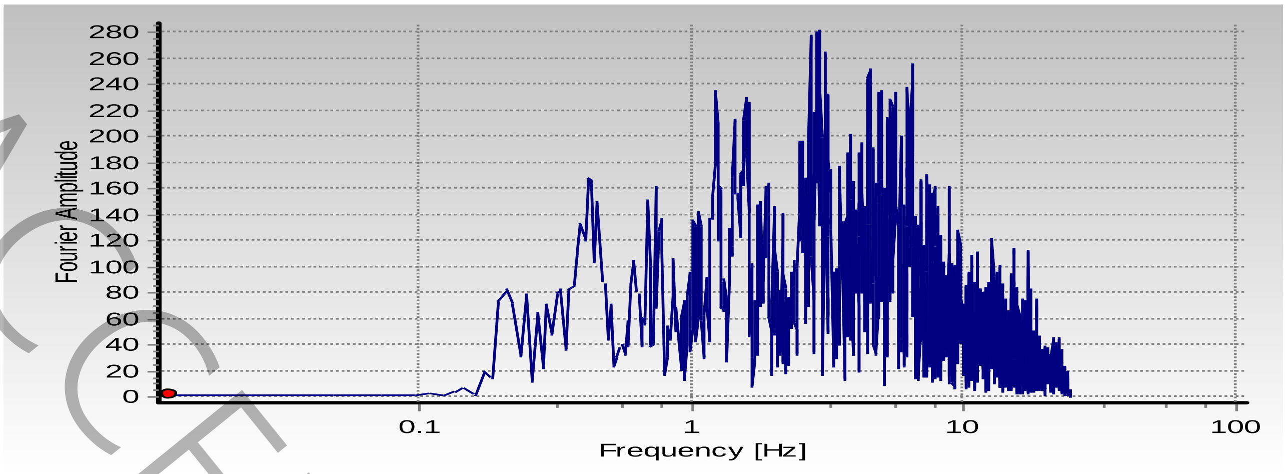

c) The Fourier function spectrum of the first component of the Manjil earthquake

Fig. 6. Acceleration of the Manjil earthquake, response acceleration, Fourier amplitude with SEISMO SIGNAL 2022 software

Since the concrete structure in contact with the soil has experienced a 0.67 reduction in strength, it is necessary to define interfaces for the entire contact surface between the concrete retaining wall and the soil, as well as in the impervious Cut-Off layer. Interfaces must also be considered for the side supports.

The boundary condition coordinates, shown in red, are defined separately in Figure 7 as follows:

The settlement results, or maximum vertical deformation under dynamic loading along the dam crest, are presented in two scenarios:

At the groundwater level upstream in the xz plane: {(0,0,0), (-20,0,0), (0,0,450), (-20,0,450)}

At the river level in the xy plane: {(0,0,0), (0,0,430), (0,-60,0), (0,-60,430)}

At the maximum reservoir level on the upstream slope: {(0,0,0), (33,99,-10), (33,99,440), (0,0,430)

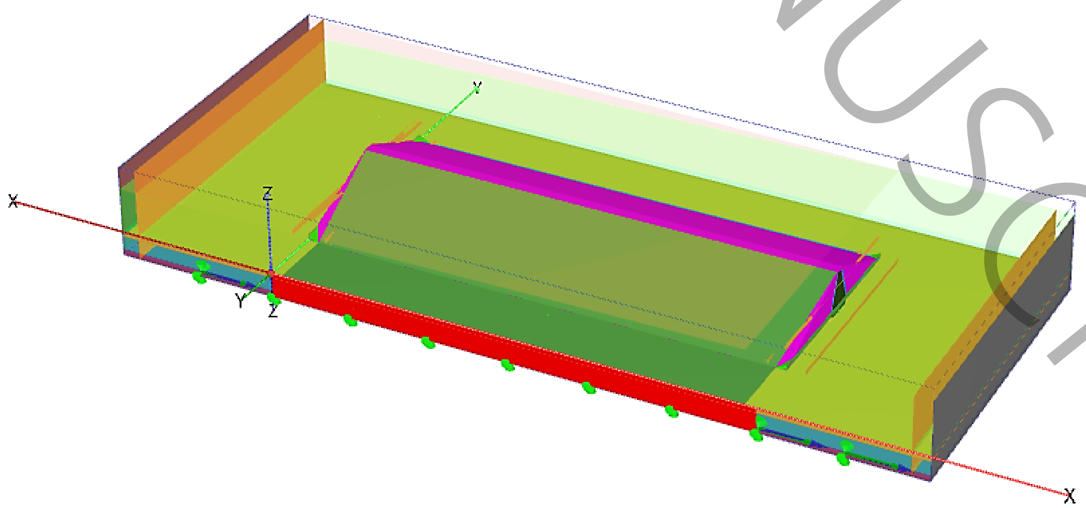

a) Groundwater level at upstream in xz plane

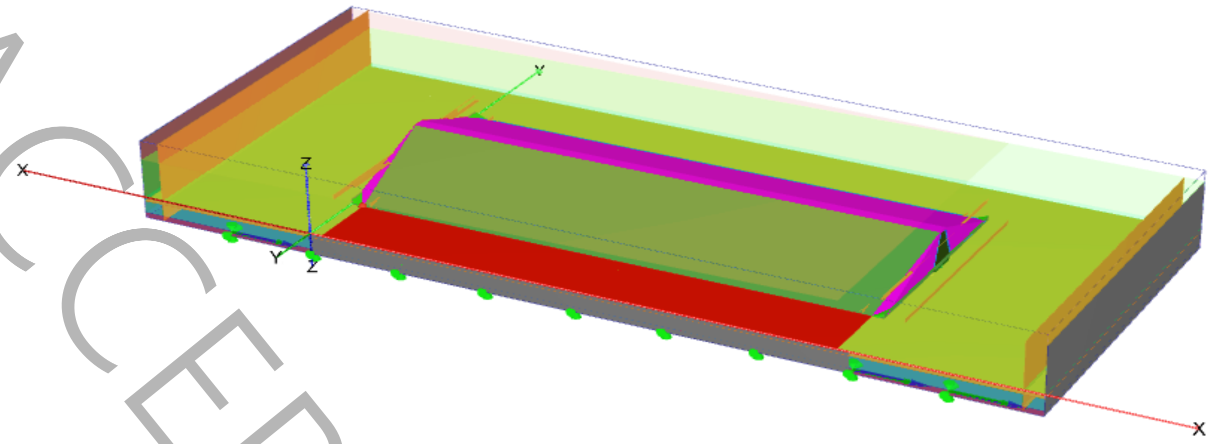

b) River level in xy plane

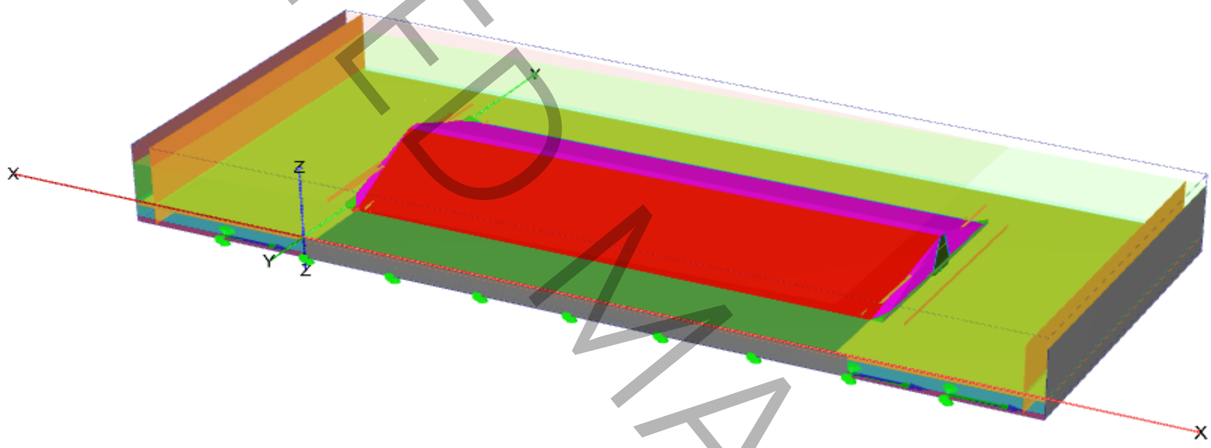

c) Maximum reservoir level on upstream slope

Figure 7: Boundary condition coordinate points

The results of settlement or maximum vertical deformation under dynamic loading along the crest of the dam are presented in two cases.

1- The maximum settlement in Figure 8, along the dam crest in the condition where the reservoir is filled to the normal level, is 0.789 meters.

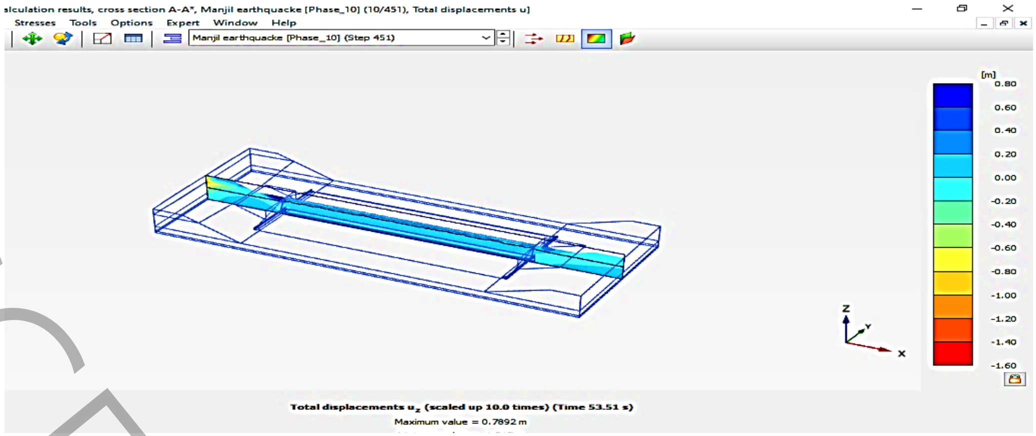

Fig. 8. The settlement along the dam crest in the case of a full reservoir

2- The maximum settlement along the dam crest, as shown in Figure 9, corresponds to the condition of a full reservoir. In the three-dimensional PLAXIS model, with the strike-slip fault taken into account, this settlement reaches 101.3 cm.

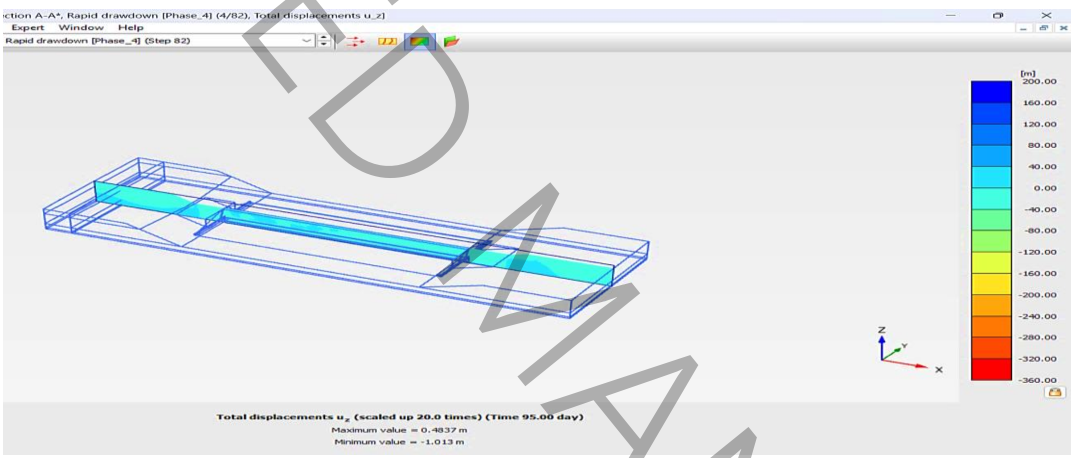

Fig.9. Impact of a strike-slip fault on the increase of settlement at the crest of an earth dam

The settlement analysis along the dam crest was examined for all 13 different phases. Two scenarios of maximum settlement or vertical deformation are presented in Figures 8 and 9. Furthermore, in the 13-phase analysis, the factor of safety obtained from the 3D PLAXIS model ranges from 1.42 to 1.85, which is fully in compliance with the standards outlined in Publication No. 624: Guidelines for Seismic Analysis and Design of Earth and Rockfill Dams.

4-Field Surveys and Ground Mapping

Following the completion of dam construction in 1999, a ground survey was conducted in 2012 along the dam crest (as shown in Figure 10). The dam was commissioned in 1999. After several years, in 2012, a monitoring campaign was conducted to assess settlement along the dam crest. The results, presented in Figure 10, revealed non-uniform settlement across the crest. However, no systematic monitoring was carried out by the operating team during this period to accurately track or analyze the settlement behavior. This significant settlement is most likely attributed to the influence of geological faults located near the left abutment of the dam site. Subsequently, a second phase of ground surveying was carried out in 2024. However, the data obtained from this phase were not used as a comparative reference, as between the two surveys, the Mazandaran Regional Water Company had carried out gravel filling, leveling, and repair works along various sections of the earth dam crest. These interventions altered the surface conditions of the crest, making a direct comparison between the 2024 data and the 2012 results invalid.

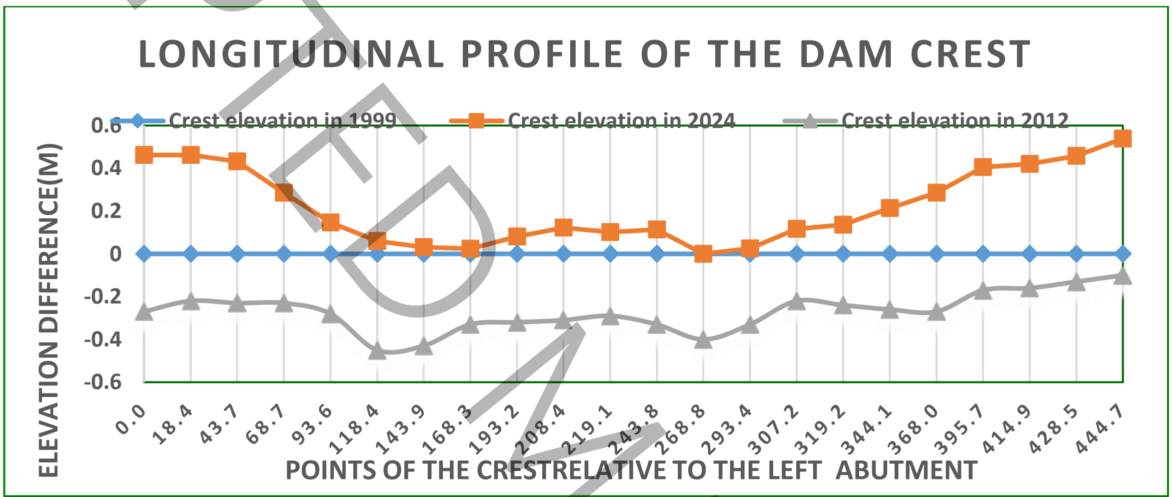

Fig.10. Comparison of Ground survey from 1999 with 2012

Figure 11 illustrates a comparison of the positions of micro-geodetic points on the downstream slope of the dam, obtained through high-precision ground-based surveying with millimeter-level accuracy. In this figure, the horizontal axis represents the distance from the edge of the dam crest toward the downstream slope, while the vertical axis shows the local elevation codes of various points along the dam body.

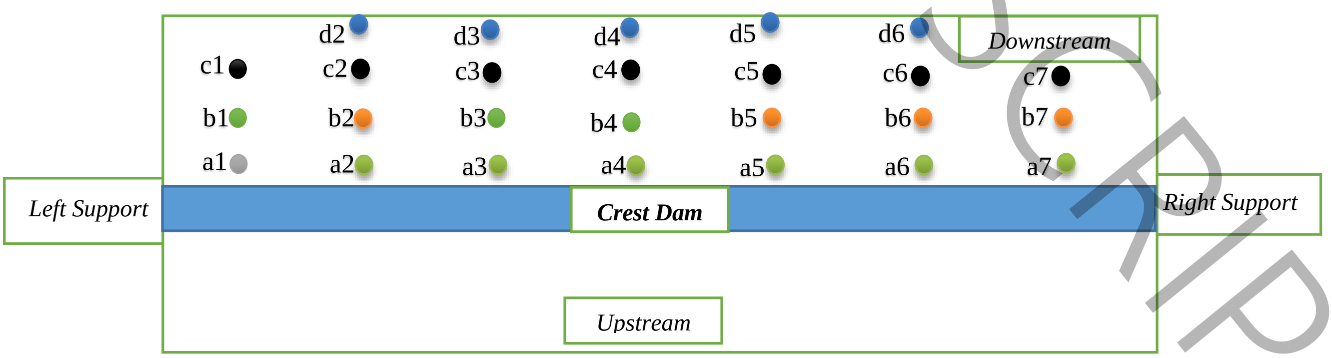

Fig.11. Positioning of micro geodetic points in the downstream slope of the Shiadah earth dam

The results clearly indicate the occurrence of uplift or swelling in the downstream slope of the dam over the period from 1999 to 2024. The swelling has been measured to be at least between 20 centimeters and 40 centimeters (Figure 12).

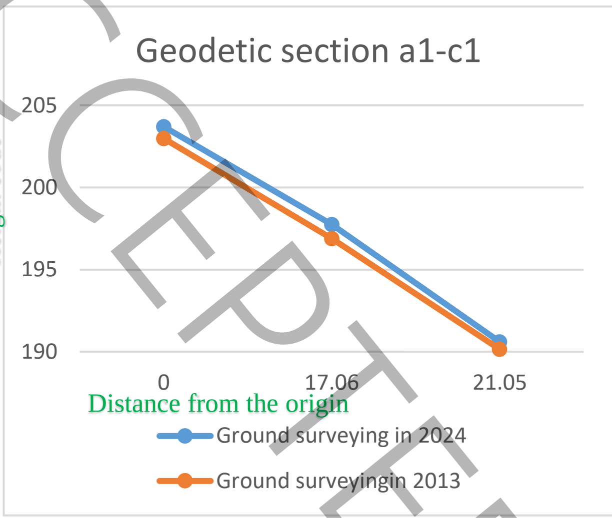

a) Geodetic section a1-c1

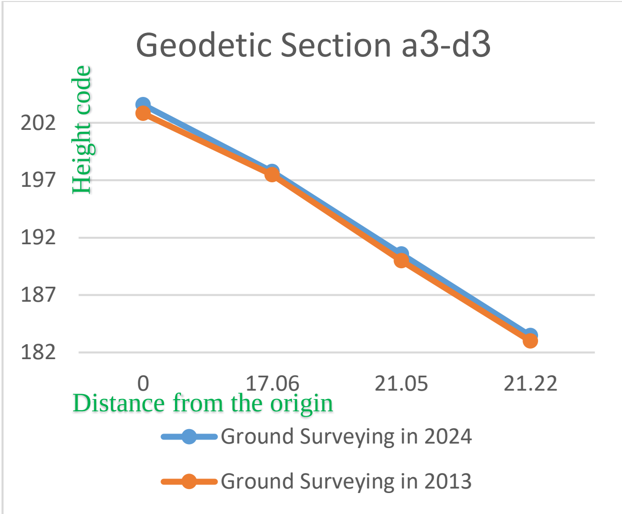

c) Geodetic section a3-d3

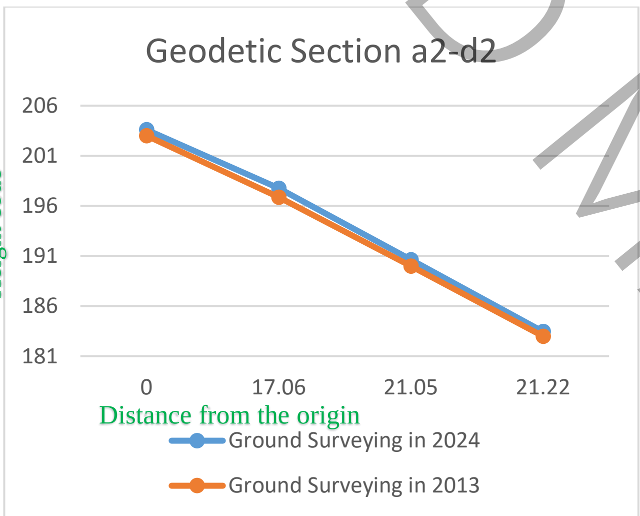

b) Geodetic section a2-d2

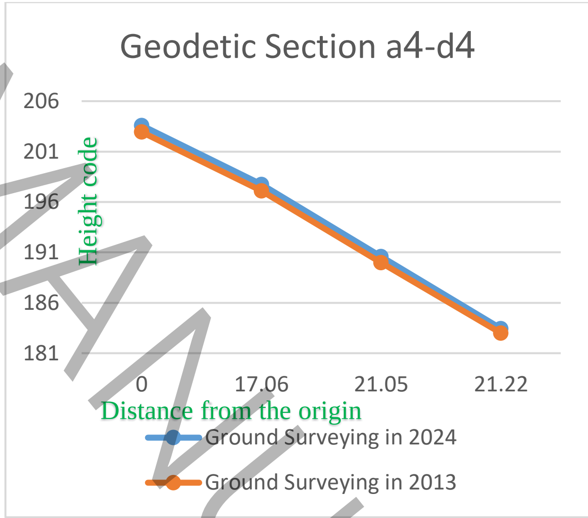

d) Geodetic section a4-d4

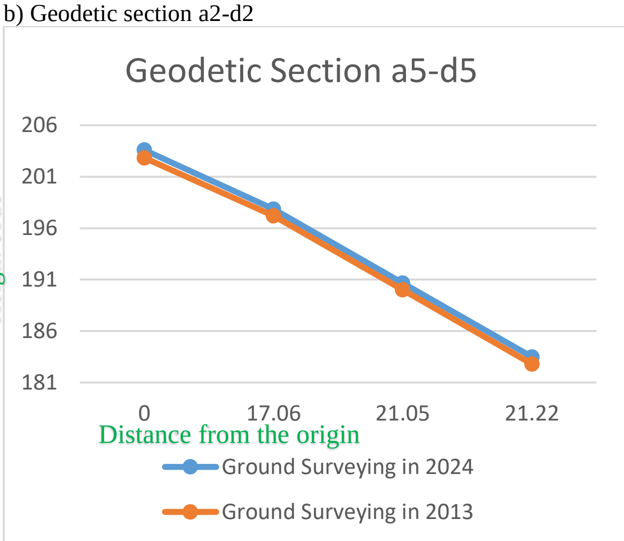

e) Geodetic section a5-d5

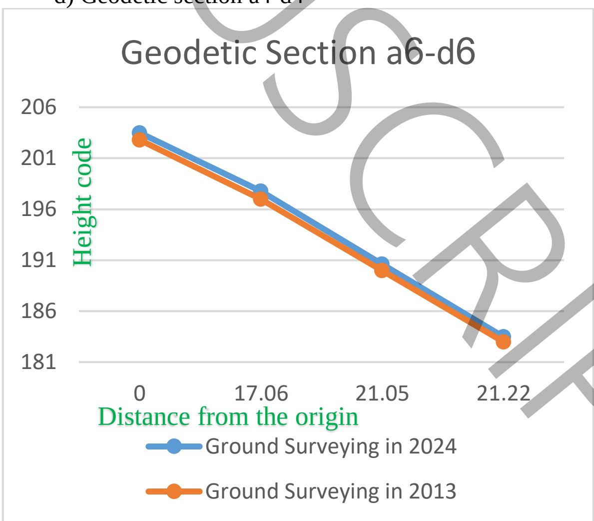

f) Geodetic section a6-d6

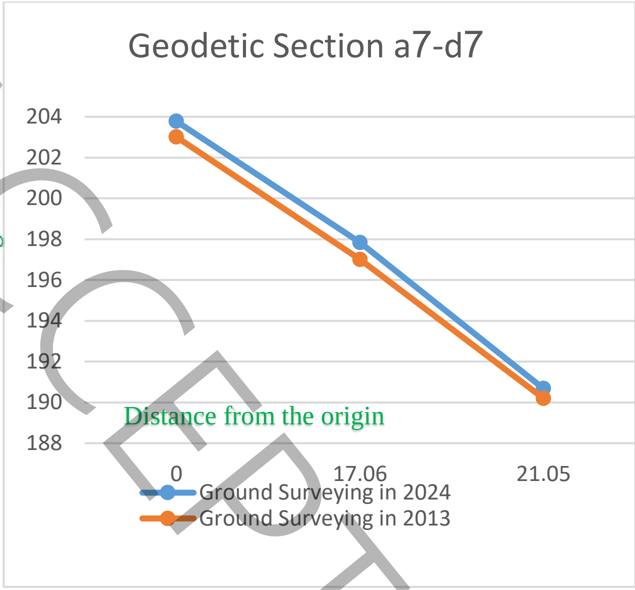

g) Geodetic section a7-d7
Fig.12. Shows several cross-sections of the micro geodetic points, clearly demonstrating the swelling or uplift of the downstream slope of the earth dam

5- THE PROPOSED RADIAL BASIS FUNCTION (RBF)

The RBF (Radial Basis Function) neural network is a type of artificial neural network known for its simplicity and strong generalization capabilities, making it effective for data prediction and function approximation tasks. Here are some of the key applications and characteristics of this neural network in data prediction:

1. Three-layer Structure: RBF networks typically consist of three layers: an input layer, a hidden layer (with nodes that use radial basis functions), and an output layer.

2. Radial Basis Functions: The nodes in the hidden layer use functions such as Gaussian or multiquadric functions, which change values based on the distance from the center of the node. This allows the network to model nonlinear relationships between data points.

3. Faster Training: Compared to multilayer perceptrons (MLP), RBF networks usually train faster because their parameters are trained locally.

Applications of RBF Neural Networks in Data Prediction are as follows:

1. Time Series Prediction: RBF networks are widely used for time series forecasting, such as stock price prediction, energy demand forecasting, and weather condition prediction. Their structure can effectively learn complex and nonlinear patterns in data.

2. Engineering and Scientific Predictions: These networks are used in tasks like predicting the behavior of structures under loads or analyzing scientific data (e.g., temperature or pressure forecasting).

3. Economic and Marketing Forecasting: RBF networks can be applied for economic trend prediction, consumer behavior analysis, and demand modeling for products.

4. Medical Predictions: In the medical field, RBF networks are utilized for predicting treatment outcomes, analyzing biological signals like ECG, and forecasting disease occurrences.

5-1-Simulation

In Table 2, the elevation code of the instrumentation for the installation on the downstream slope of the Shiadah earth dam is shown for settlement measurement. During the years when the instrumentation was functioning properly, a total of 530 data entries related to settlement were recorded, which served as the basis for settlement prediction calculations using the RBF algorithm.

Table 2. The elevation code of the instrumentation

Precision tools axis A	Install level	Precision tools axis B	Install level	Precision tools axis C	Install level
A1	179.6	B1	178	C1	176.25
A2	180.11	B2	178.51	C2	178.9
A3	182.75	B3	181.27	C3	182.51
A4	186.42	B4	185.07	C4	186.19
A5	190.19	B5	188.83	C5	189.84
A6	193.98	B6	196.38	C6	-

Initially, the settlement prediction for instrumentation A1 at level 179.60 was carried out using 530 recorded data entries in MATLAB R2019a software, and after analysis, the settlement results are presented in Figure 13.

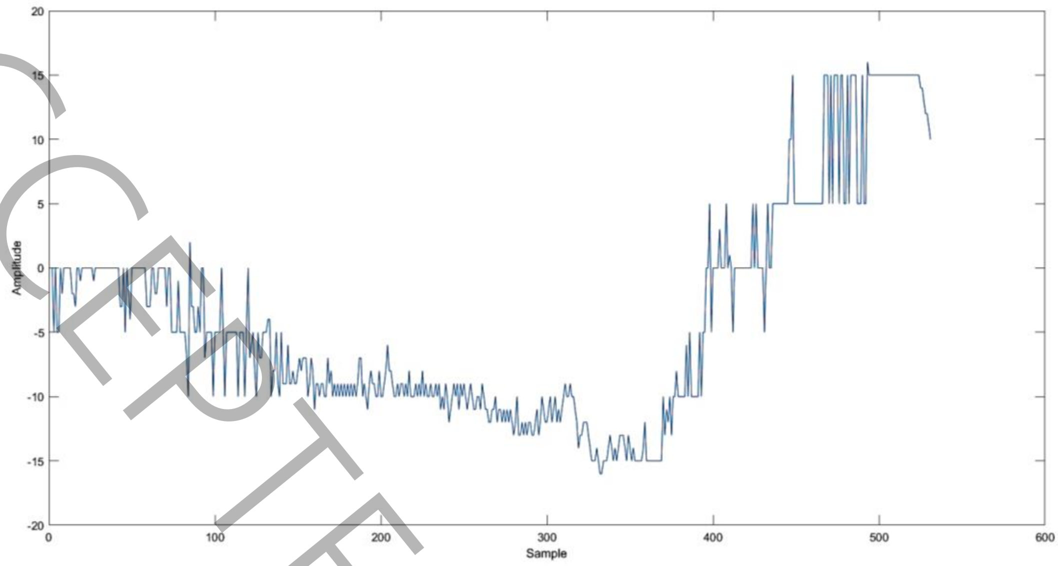

Fig. 13. Settlement data

To predict the settlement for the year 2024, a customized program was developed in MATLAB to simulate and reproduce the settlement trend by considering the historical pattern from 1999 to 2012. As a result of this modeling process, the predicted settlement for 2024 was obtained and is shown in red in Figure 14.

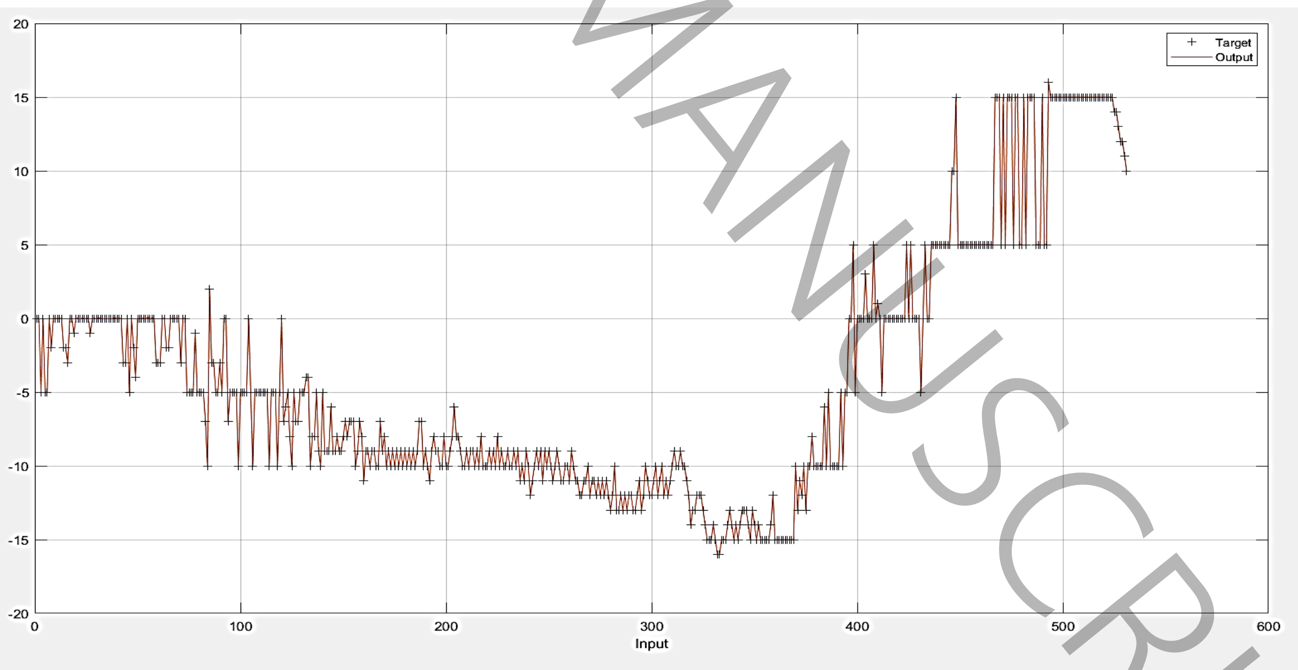

Fig.14. Prediction of settlement data with the RBF neural network in red

Enter the Error value and Error Spread constant, and after running the code, the network begins training to fit the existing data. With the completion of the training process, as shown in Figures 15 and 16, it can reach the desired error level.

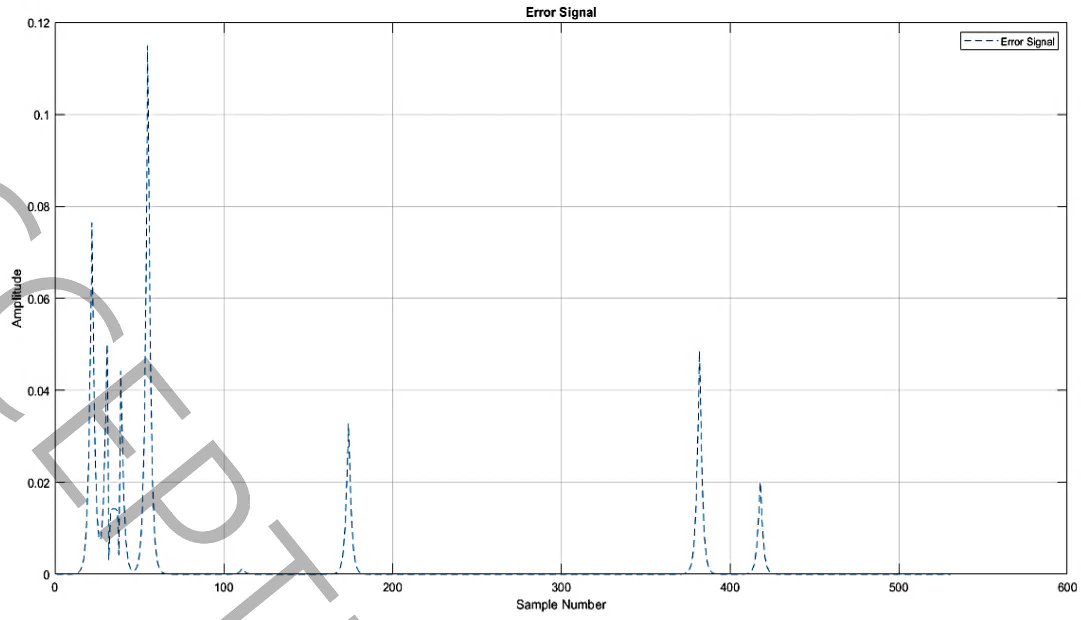

Fig. 15. Error function

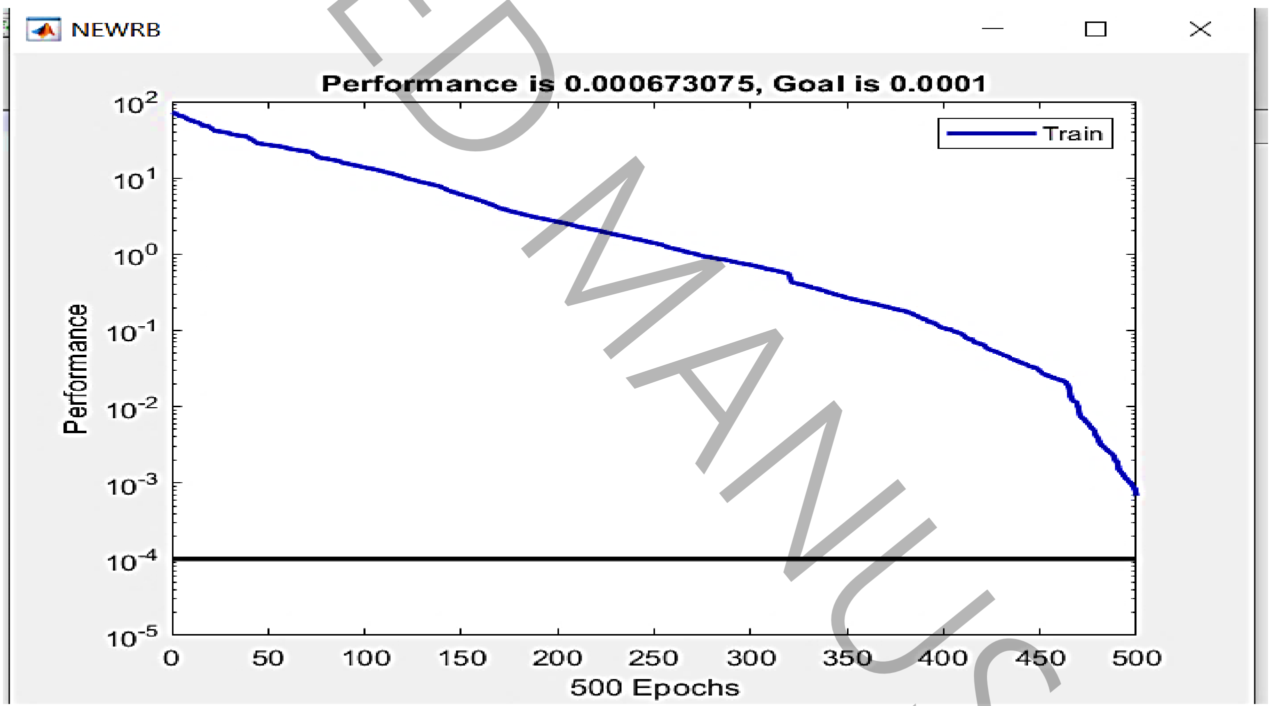

Fig. 16. Improvement of neural network performance

The data, following the target output we aim for from the network, shows in Figure 17 that the neural network can predict the time series, meaning it is fully adaptable and demonstrates a good fit with the data.

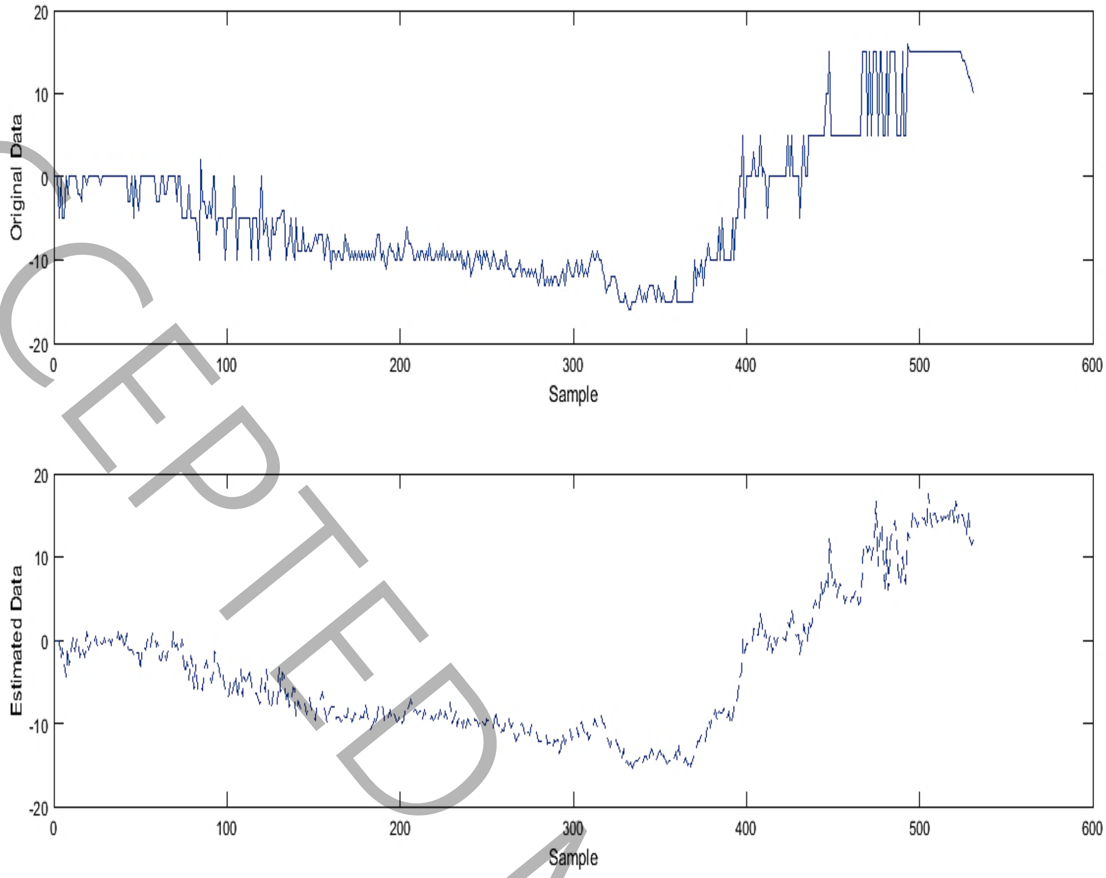

Fig.17. Suitable adaptability and fit of the network output

The neural network was trained with the existing 530 data points, as shown in Figure 18, enabling prediction of the next data point. To predict new data points, the following command is used.

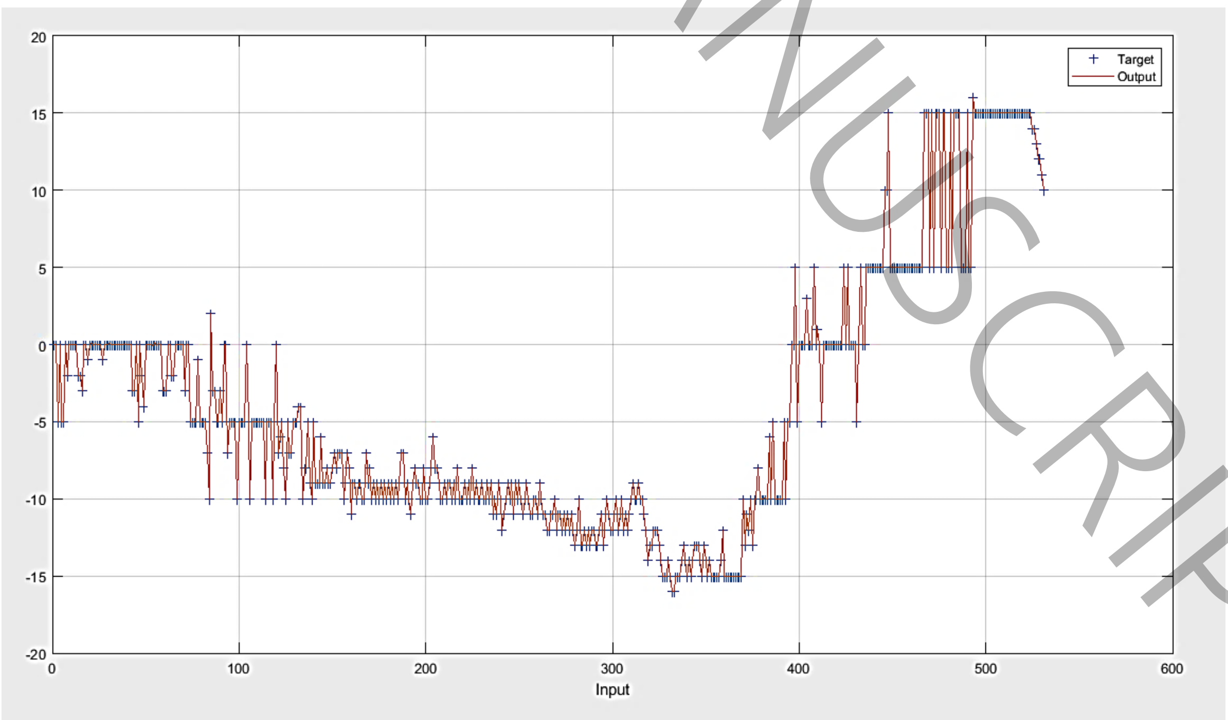

Fig.18. System modeling using an neural network

In this command, X represents the input, net is the network, and Y is the output. The results of the prediction are displayed in the following figure. It is worth mentioning that the number of input data to the network can be adjusted by the user. For example:

```
X2 = 531:531;
Y2 = sim (net, X2);
hold on
plot (X2, Y2, '*')
```

Based on the output and results obtained from the neural network system, as shown in Figure 19, the predicted value is indicated as 10 mm by an asterisk (*).

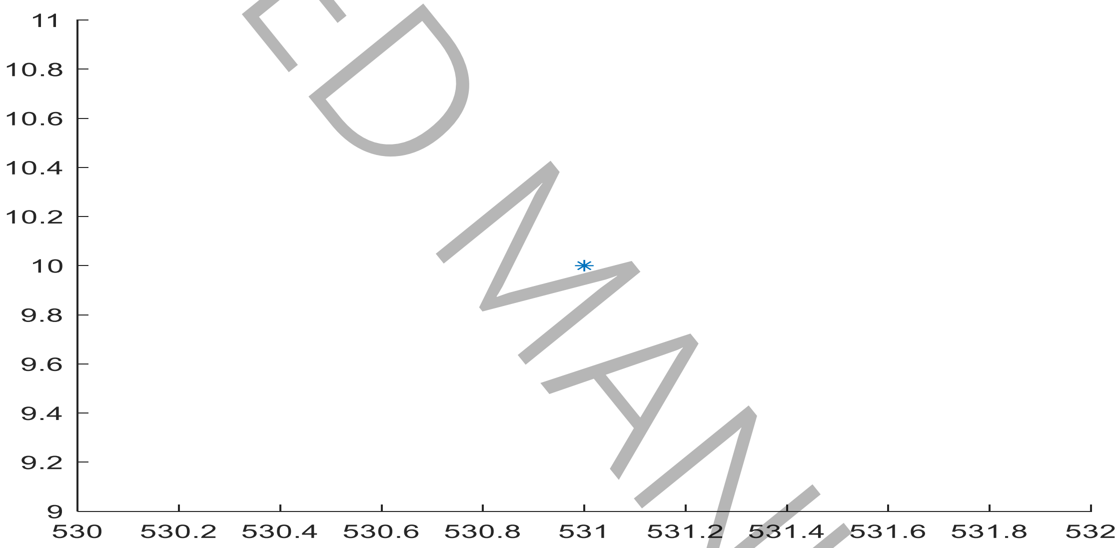

Fig.19. Prediction results from the neural network system

In Table 3, a summary of the predicted settlement values in millimeters using the neural network is provided for the instrumentation installed at cross-section A-A on the downstream slope, located 120 meters from the left abutment of the dam.

Table 3. Predicted settlement results of instrumentation using the RBF neural network

Elevation code of the installed instrumentation	Prediction of settlement value using the neural network (mm)
A1 (179.60)	10
A2 (180.11)	-13
A3 (182.75)	-18
A4 (186.42)	-19
A5 (190.19)	-15
A6 (193.98)	-5

In Table 4, a summary of the predicted settlement values in millimeters using the neural network is provided for the instrumentation installed at cross-section B-B in the middle section of the downstream slope, located 220 meters from the left abutment of the dam.

Table 4. Predicted settlement results of instrumentation using the neural network

Elevation code of the installed instrumentation	Prediction of settlement value using the neural network (mm)
B1 (178. 0)	8
B2 (178.51)	-8
B3 (181.27)	-18
B4 (185.04)	-37
B5 (188.83)	-35
B6 (196.33)	-2

In Table 5, a summary of the predicted settlement values in millimeters using the neural network is provided for the instrumentation installed at cross-section C-C on the downstream slope, located 318.52 meters from the left abutment of the dam.

Table 5. Predicted settlement results of instrumentation using the neural network

Elevation code of the installed instrumentation	Prediction of settlement value using the neural network (mm)
C1 (176.24)	15
C2 (178.9)	-8
C3 (182.53)	-27
C4 (186.19)	-31
C5 (189.84)	-24

In this study, the performance of two machine learning models—Radial Basis Function (RBF) neural network and Support Vector Machine (SVM) with RBF kernel—was compared on a specific dataset. The results indicate that the RBF network achieved superior accuracy, with a Root Mean Square Error (RMSE) of 0.0100, Mean Absolute Error (MAE) of 0.0025, and a coefficient of determination (R2)=1.0000, indicating an almost perfect fit to the target data. In contrast, the SVM model yielded an RMSE of 2.2612, MAE of 1.3287, and R2=0.9289, demonstrating comparatively lower predictive accuracy as shown in Table 6.

This significant performance gap can be attributed to several factors. Primarily, the nature of the dataset appears to be smooth, continuous, and characterized by very low noise. The RBF network, utilizing radial basis functions, is inherently well-suited for approximating smooth and continuous functions, enabling it to closely model the underlying data patterns with minimal error.

On the other hand, the SVM with RBF kernel relies heavily on proper tuning of hyperparameters such as the regularization parameter CCC and the kernel width parameter γ\gammaγ. Without rigorous hyperparameter optimization, the SVM's ability to generalize accurately is compromised, likely explaining the observed performance drop. Moreover, SVMs typically exhibit better robustness in noisy data scenarios or when decision boundaries are complex; however, in this case, where the data structure is relatively simple and smooth, the RBF network's approximation capability proves more effective.

Furthermore, dataset size and dimensionality also play a crucial role in model selection. The RBF network's relatively simple architecture and faster training time make it particularly suitable for small to medium-sized datasets with low-dimensional input features. Conversely, SVMs, although computationally more intensive, can provide better generalization in large-scale and high-dimensional problems, provided that hyperparameters are carefully optimized.

In conclusion, these findings highlight the importance of considering data characteristics and model tuning when selecting an appropriate learning algorithm. The RBF network, due to its simplicity and high accuracy in approximating smooth, low-noise data, emerged as the preferred model for the present task. However, for more complex and noisy datasets, thorough hyperparameter optimization of SVMs may yield superior performance.

Table 6. Comparision of RFB and SVM

Performance Metric	RBF Network	SVM (RBF Kernel)
Root Mean Square Error (RMSE)	0.01	2.261
Mean Absolute Error (MAE)	0.0025	1.3287
Cofficient of Determination (R^2)	1.0	0.9289

1. Training–testing data separation:

The complete dataset was randomly divided into training and testing subsets using an 80:20 ratio. Specifically, 80% of the data were used for model training, while the remaining 20% were reserved exclusively for independent testing. The testing dataset was not involved in the model development or parameter optimization stages.

2. Cross-validation procedure:

To further evaluate the robustness and stability of the proposed RBF model, a 5-fold cross-validation method was implemented. In this approach, the dataset was divided into five equal subsets, and the model was trained and validated iteratively using different combinations of the subsets. The average validation performance obtained from the cross-validation process showed consistent and stable results, confirming the reliability of the model.

3. Performance metrics in training and validation stages:

The revised manuscript now reports separate statistical indicators for both training and testing datasets. The obtained results are as follows:

- Training dataset: $R^2 = 0.9987$, RMSE = 0.012
- Testing dataset: $R^2 = 0.9924$, RMSE = 0.021

Although the prediction accuracy remains high, the slight reduction in the testing performance compared with the training stage demonstrates that the model maintains strong predictive capability without severe overfitting.

4. Discussion on overfitting and generalization:

An additional discussion has been included in the revised manuscript regarding model overfitting and generalization ability. The close agreement between the training, testing, and cross-validation results indicates that the proposed RBF model has satisfactory generalization performance and can reliably predict unseen data within the investigated domain.

These revisions significantly improve the transparency and credibility of the proposed modeling framework.

6- Conclusion

The Shiadeh Earth Dam was first impounded in 1999. A comparison of the dam's settlement from 1999 to 2012, measured at a distance of 118.4 meters from the left abutment, revealed the highest recorded settlement during this period. Additionally, a 3D analysis conducted using PLAXIS software, considering all impoundment phases and static and dynamic loading conditions with an appropriate safety factor, estimated a total settlement of 78.09 centimeters.

Considering the effect of the strike-slip fault at the normal reservoir water level, the maximum vertical settlement at the crest of the Shiadeh earth dam was estimated to be 101.3 cm. The results clearly demonstrate that the presence of this fault has led to an intensification of settlement along the dam crest. In the three-dimensional numerical modeling using PLAXIS software, all geotechnical parameters including elastic modulus, cohesion, internal friction angle, and permeability were directly obtained from Table 1, which summarizes the results of field and laboratory tests conducted on eight boreholes. In this study, field visits and ground surveys of microgeodetic points and the crest of the earth dam were conducted. The results clearly indicate the occurrence of uplift or swelling in the downstream slope of the dam over the period from 1999 to 2024. The swelling has been measured to be at least between 20 centimeters and 40 centimeters.

By combining, the accuracy of numerical modeling, the predictive power of advanced algorithms, and field validation, a comprehensive and reliable early warning system can be designed—one that serves as an effective step toward enhancing the safety of the country's water infrastructure.

It is recommended that this category of dams be entrusted to a multidisciplinary research team (including geotechnics, geology, crisis management, economics, and programming). Therefore, completing geological and geotechnical studies is essential to determine the slope of the foundation soil layers and fault fractures to assess potential water leakage from the reservoir. Additionally, the destructive impact of secondary faults from a geological perspective must be thoroughly investigated.

Acknowledgment

Dr.Seyed Mahmoud Anisheh is acknowledged in this research for his contributions to the algorithm calculations and for his wholehearted cooperation.

References

[1] Beiranvand, B., Komasi, M. (2024). Spatiotemporal clustering of dam settlement monitoring using instrumentation data (case study: Eyvashan Earth Dam). Results in Engineering 22 (2024) 102014

[2] Ghosh, B. Kumar, V. (2023). Calibration & Prediction of Seismic behaviour of CFRD dam for Performance Based Design. 30 October 2023.

[3] De Alba P, S. H. B. M. F. I. &. (1978). Performance of earth dams during earthquakes.

[4] Seed, H. B. (1979). Considerations in the earthquake-resistant design of earth and rockfill dams.

[5] Javdanian, H. Zarei, M. Shams, G. (2023). Estimating seismic slope dis-placements of embankment dams using statistical analysis and numerical modelling. Modelling Earth Syst Environ 9(3):389–396. https://doi.org/10.1007/s40808-022-01505.

[6] Javdanian, H. Pradhan, B. (2019). Assessment of earthquake-induced slope deformation of earth dams using soft computing techniques. Springer Berlin Heidelberg

[7 Chen, G., Jin, D., Mao, J., Gao, H., Wang, Z., Jing, L., Li, Y., & Li, X. (2014). Seismic damage and behavior analysis of earth dams during the 2008 Wenchuan earthquake, China. Engineering Geology, 180,99–129. https://doi.org/10.1016/j.enggeo.2014.06.001.

[8] Jamaludin, M., Mahadzir, M., Abu Karim, A. (2022). Structural performance observation of the earth

dams in Pulau Pinang using a vibrating wire piezometer and surface settlement marker.

[9]Ambraseys, N. N. and Sarma, S. K. (1967). The response of earth dams to strong earthquakes', Geotechnique.

[10] Idriss, I. M. J. Mathur, M. Seed, H. Bolton. (1973). Earth Dam-foundation interaction during earthquakes. https://doi.org/10.1002/eqe.4290020403

[11] Beiranvand, B., Komasi, M. (2021). An investigation on dam settlement during and end of construction using instrumentation data and numerical analysis. SN Appl. Sci. 3 (3) (2021), https://doi.org/10.1007/s42452-021-04306-z.

[12] Bray, J.D., Macedo, J., and Travasarou, T. (2017). Sim-plied procedure for estimating seismic slope displacements for subduction zone earthquakes. Journal of Geotechnical and Geoenvironmental Engineering, 144(3), 04017124

[13] Li, Y. Min, K. Zhang, Y. Wen, L. (2021). Prediction of the failure point settlement in rockfill dams based on spatial-temporal data and multiple-monitoring-point models. Eng. Struct. 243 (112658) (2021) 112658, https://doi.org/10.1016/j. engstruct.2021.112658.

[14] Cao, W. Wen, Z. Su. H. (2023). Spatiotemporal clustering analysis and zonal prediction model for deformation behavior of superhigh arch dams. Expert Syst. Appl. 216 (2023) 119439, https://doi.org/10.1016/j.eswa.2022.119439, 119439.

[15] Wang, J. Gu, H. Chen, B. Gu, C. Zhang, Q. Xing, Z. (2021). A spatiotemporal dam deformation zoning method considering nonuniform distribution of monitoring information. IEEE Access: Pract. Innovat. Open Solut. 9 (2021) 117615–117628, https://doi.org/10.1109/access.2021.3106817.

[16] Hu, J. Ma. F. (2020). Zoned deformation prediction model for super high arch dams using hierarchical clustering and panel data. Eng. Comput. 37 (9) (2020) 2999–3021, https://doi.org/10.1108/EC-06-2019-0288.

[17] Chen, B. Hu, T. Huang, Z. Fang, C. (2019). A spatiotemporal clustering and diagnosis method for concrete arch dams using deformation monitoring data. Struct. Health Monit. 18 (5–6) (2019) 1355–1371, https://doi.org/10.1177/1475921718797949.

[18] Suprijanto, H. Sayekti, R W. Pratama, R R. Wiyata, F A. (2024). Potential deformation assessment of Semantok Main Dam in North Nganjuk Region at East Java Indonesia. IOP Conf. Series: Earth and Environmental Science. 1311 (2024) 012008. doi:10.1088/1755-1315/1311/1/012008

[19] Antonio Morales-Esteban 1, José Luis de Justo Alpañés. (2024). Dynamic Analysis of the Almagrera Tailings Dam with Dry Closure Condition. Sustainability 2024, 16, 1607. https://doi.org/10.3390/su16041607

[20] Kong, X. J., Pang, R., Zou, D. G. Xu, B., Zhou, Y. (2018). Seismic performance evaluation of high CFRDs based on incremental dynamic analysis.

[21] Ding, Y., Wan, H. P., and Wang, S. (2023). Settlement prediction of existing metro induced by new metro construction with machine learning based on SHM data: a comparative study. Journal of Civil Structural Health Monitoring, vol. 13, no. 2-3, pp. 579-589, 2023.

[22] Jagan, J., Samui, P., and Kim, D. (2023). Reliability analysis of simply supported beam using GRNN, ELM and GPR. Structural Engineering and Mechanics. vol. 71, no. 6, pp. 000-000, 2023.

[23]Wang, F., Gou, B., and Qin, Y. (2023). Modeling tunneling-induced ground surface settlement development using a wavelet smooth relevance vector machine. Computers and Geotechnics. vol. 54, pp. 125-132, 2023.

[24] Zhang, X., Li, Y. and Zhao, W. (2024). Analysis and prediction of compressive and split-tensile strength of secondary steel fiber reinforced concrete based on RBF fuzzy neural network model. PLoS One, vol. 15, no. 1, pp. 1-10, Feb. 2024. DOI: 10.1371/journal.pone.0299149.

[25] Wang, H. Sun, J. and L. Liu (2024). A hybrid RBF neural network based model for day-ahead prediction of photovoltaic plant power output. Frontiers in Energy Research. vol. 8, no. 2, pp. 1-12, Mar. 2024. DOI: 10.3389/fenrg.2023.00125

[26] Anisheh, S. R., Anisheh, S. A., & Anisheh, S. H. (2019). Seismic analysis of Narmab earth dam and optimization of its parameters using cuckoo. In Sustainable and Safe Dams Around the World (pp. 2875–2883). CRC Press.

[27] Farrokhi, F., Rasouli, R., Anisheh, S.R . (2018). Seismic Analysis of Homogeneous Earth Dam and Optimization of Its Parameters Using Pso. Internatıonal Journal of Natural and Engineering Sciences E-ISSN: 2146-0086 12 (1): 42-48, 2018

[28] Anisheh, S. R. Anisheh S. M. (2012). Application of Finite Difference Method and PSO Algorithm in Seismic Analysis of Narmab Earth Dam. International Journal of Computer Applications, Vol. 54, pp. 1-5, New York, 2012.

[29]Anisheh, S. R. Sarifipour. M. (2024). Optimization of the effective width of the foundation of a homogeneous earth dam under earthquake using the IWO algorithm. Internatıonal Journal of Natural and Engineering Sciences E-ISSN: 2146-0086 18 (2): 77-91, 2024.

[30]Khoshraftar (2019). Evaluation of the relationship between faults and karst springs in the Bisotun mountain massif, Kermanshah.

[31] Report "Geotechnical studies of Shiadeh reservoir site - second phase studies - Shiadeh Reservoir Dam", consultant Khazar Ab (1998).

[32] Report of the Shiadeh Dam Project, Regional Water Company of Mazandaran Province, (1998).

[33] The phase 2 studies of the technical studies Report of the Shiadeh Dam", consultant Khazar Ab (1998).

[34] The Mazandaran Regional Water Company Control and Stability Report, (1999-2013)

[35] Babol water Resources Affairs,affiliated with the Mazandaran Regional Water Company (1999-2024)